Natural and Applied Sciences International Journal (NASIJ)
eISSN: 2788-4619 (online)
https://ideapublishers.org/index.php/nasij
Vol. 6, No. 1 (January-June), 2025, pp. 1-28
https://doi.org/10.47264/idea.nasij/6.1.1
Original Research Article

Neurodynamic analysis of NACA 0012 airfoil and wing using Bayesian regularisation

Mamoon Aamir[1] | Husnain Raza Qasim[2]

1. Department of Aeronautics and Astronautics, Institute of Space Technology, Islamabad, Pakistan.
2. Faculty of Engineering, Emirates Aviation University, Dubai, United Arab Emirates.

* Corresponding Author Email: mamoonaamir08@gmail.com

Abstract:

This paper proposes a novel neural network-based approach with Bayesian regularisation for analysing air foils and wings. Here, the established NACA0012 airfoil, a standard in aviation and aerospace engineering, is used. Empirical methods, various software, and computational fluid dynamics (CFD) simulations have been commonly employed in airfoil analysis. To forecast and model the aerodynamic characteristics of the NACA0012 airfoil and its wing counterparts, this study presents a data-driven approach utilising artificial neural networks (ANNs). Datasets are first generated using software xflr5, followed by AI-based Bayesian regularisation (AI-BR). Approximations in analyses were demonstrated using three data sets: training (80%), testing (10%), and validation (10%), with 20 neurons. Large-scale Simulink results on mean-squared error, error histograms, and regression analyses further emphasise the proposed AI-BR's competence, dependability, and accuracy. A direct and immediate way to assess the accuracy of models or measurements is to use an absolute error (AE) plot, which shows the differences between estimated and actual values. The findings support the effectiveness of integrating ANNs with Bayesian regularisation in aerodynamic analysis. The approach not only enhances prediction accuracy but also opens new avenues for future investigations into more complex aerodynamic models.

Article History

Received:
10-Apr-2025

Revised:
10-May-2025

Re-revised:
18-Jun-2025

Accepted:
20-Jun-2025

Published:
30-Jun-2025

Keywords: Computational intelligence, Fluid dynamics, Aerodynamics, Data-driven analysis, Artificial neural network, Artificial intelligence.

How to Cite: Aamir, M. & Qasim, H. R. (2025). Neurodynamic analysis of NACA 0012 airfoil and wing using Bayesian regularisation. *Natural and Applied Sciences International Journal (NASIJ), 6*(1), 1-28. https://doi.org/10.47264/idea.nasij/6.1.1

1. Introduction

Wing and airfoil research are critical in understanding and enhancing aircraft performance. To ensure that aircraft yield the correct lift and show the proper flying behaviour, aerodynamicists and engineers inspect airfoil shapes, angles of attack, and other design considerations in minute detail. This research plays a crucial role in ensuring the safe and successful operation of all types of aircraft, including high-performance military aircraft and commercial airliners. The size of an airfoil and a wing relative to an aircraft is primarily what distinguishes them from each other. A specific cross-sectional shape, frequently streamlined, designed to manage airflow and generate lift, is known as an airfoil. It is an essential component of a wing, as well as other aerodynamic structures such as helicopter rotor blades or propeller blades. To efficiently generate lift, minimise drag, and provide stable flight behaviour, airfoils are researched and constructed. A wing, however, constitutes the entire lifting surface of an aircraft. It is a larger structure comprising numerous airfoils that often covers the entire length of the aircraft. To supply the total lift needed to sustain the aeroplane in flight, the wing uses many different airfoil shapes, attack angles, and structural elements.

Ailerons, flaps, and winglets are other features that wings incorporate to control and optimise performance in different stages of flight. Essentially, a wing is the entire lifting structure of an aircraft that contains numerous airfoils and other features necessary for controlled and efficient flight. However, an airfoil can be a particular component of a wing. Experimental measurement is the topic of recent works on unmanned aerial vehicles (UAVs) wherein wings have different aerodynamic characteristics based on the chord Reynolds number or aspect ratio. Yet, the typical shortcoming of backpropagation training in traditional ANNs is overfitting, wherein the network performs exceptionally well on the training data but fails to extend to new cases. The aerodynamic performance in terms of maximum lift, lift curve slope, and polar curves is also quite interesting (Ananda *et al.*, 2015). UAVs often operate in the 50,000–150,000 chord Reynolds number range.

The research of 3D shape-change and optimisation frameworks, where the aspect ratio significantly influences performance, is also quite popular (Boulkeraa *et al.*, 2014; Fincham & Friswell, 2015). This is the driving force behind our experimental investigation, which aims to investigate the aerodynamic properties at low to moderate Reynolds numbers, thereby comparing our findings with those of earlier studies that used different aspect ratios. A surface with the least amount of drag and the most lift is called a wing profile. The aerodynamic characteristics of the wing cross-section control the relationship between the two forces (Abbott & von Doenhoff, 1959). The majority of these computational and experimental experiments focused exclusively on evaluating flow dynamics. Therefore, C_D and C_L coefficients take into account the entire fluid-structure scenario, giving us a general idea of how the wing interacts with the flow that flows over it.

The aerodynamic characteristics of the NACA 0012 airfoil have been thoroughly investigated, and large eddy simulation has been used to compare numerical results with experimental results (Cuerno-Rejado *et al.*, 2001). For various 2D airfoils, Abbot and von Doenhoff (1959) published a substantial review of experimental data. The highest C_L recorded by these authors ranged from 1.1 to 1.6 for chord-based Reynolds numbers between 3 and 9 106 and stall angles between 12° and 16°. The lift coefficient rises linearly with a constant slope C_L/ for angles less than stall. The wing surface roughness affects the minimum C_D. A 2D NACA 0012 model was evaluated by Sheldahl and Klimas (1981) two decades later for chord-based Reynolds numbers

between 3.6×10^5 and Rec 7×10^5 and AoA in the range of 0° to 180°. In contrast to Abbot and von Doenhoff's (1959) work, their findings revealed a decrease in the maximum lift coefficient (C_{Lmax}= 0.9–1.0) and the stall angle (stall =$10^{\circ} - 12°$), albeit the slope of the lift curves as a function of for small AoA was in agreement.

Sheldahl and Klimas (1981) have noted that the slope declines at AoAs larger than 5°–6°. Three-dimensional impacts on the dynamics of the wingtips are important up to a specific limit value. Additionally, due to the vortex wandering, the location of the Centre of the vortex had to be changed while taking PIV measurements (Del Pino *et al.*, 2011). In reality, wingtip vortices on finite wings cause an increase in drag coefficient as well as a drop in lift coefficient relative to a 2D infinite airfoil (referred to as "downwash"). The significance of this tendency increases as the aspect ratio decreases its value. Tests were conducted by Laitone (1997) using a rectangular finite wing with a NACA 0012 cross-section shape, AR=6, chord-based Reynolds numbers under 7104, and free-stream turbulence intensity 0.02%–0.1%. For Re_c= 2.07×10^4. and Re_c= 4.21×10^4., these results demonstrated a discontinuity in the slope of the linear area of the lift curves at tiny AoA. This discontinuity reduces as the free stream velocity rises, along with the gradual slope C_L increment. Similar to the maximum turbulence intensity, the maximum lift coefficient for a constant Reynolds number of falls. Additionally, Laitone noted that when Rec rises, the minimum drag coefficient $C_{\_Dmin}$ (null AoA) gradually decreases. The curve for the C_{Dmin} evolution with Reynolds number fits at C_{Dmin}= 0.35 Re_c-0.25. Additionally, Nngo and Barlow (2002) measured a rectangular NACA0012 (AR4) in a low-turbulence wind tunnel in order to research the mechanism that lessens the drag force brought on by the wingtip vortex for Re_c= 4.8×10^5. They found that C_{Lmax} is about 0.6 for the crucial (stall) angle stall = 11°, and that C_{Dmin}= 0.048 for 0°. These figures are examined to illustrate how the geometry (such as aspect ratio) and the presence of edge effects significantly impact the aerodynamic properties of the NACA 0012 airfoil.

Artificial neural networks (ANNs) are now advanced computational tools that can represent highly nonlinear relationships and discern patterns in intricate datasets where traditional analytical techniques tend to malfunction. With the ability to simulate parallel processing in the human brain, ANNs can approximate functions, detect hidden correlations, and generalise beyond the training set, making them highly suitable for engineering systems under nonlinear dynamics. To address this issue, Bayesian regularisation (BR) has been suggested as an effective training strategy that internally normalises the network parameters to strike a balance between model complexity and predictability. By incorporating Bayesian inference in the weight optimisation process, BR avoids overfitting and ensures that the learned network is robust even when handling sparse, noisy, or small datasets. This renders ANN-BR models highly desirable to scientific and engineering applications where experimental data are costly or computational simulations are time-intensive.

Recent studies have proven the efficacy of such neuro-computing methods in several disciplines, like prediction of heat transfer, fluid-structure interaction modelling, diseases and cryptographic networks (Abbasi *et al.*, 2025a; Abbasi *et al.*, 2025b; Aamir *et al.*, 2025; Chen *et al.*, 2025; Sabir *et al.*, 2025; Karay *et al.*, 2025) as well as aerodynamics (Anand *et al.*, 2025; Camacho *et al.*, 2025; Wassing *et al.*, 2025). Regardless of these improvements, the use of ANN with Bayesian regularisation for aerodynamic performance prediction, particularly for extensively studied benchmark airfoils like NACA0012, remains untapped. This shortage highlights the need for more studies to evaluate the prospects of ANN-BR structures as viable surrogates of conventional CFD or experimental methods in aerodynamic analysis. Unlike

previous studies that relied mainly on CFD or experiments, this study suggests a neurocomputing-based Bayesian regularisation method for aerodynamic prediction with enhanced accuracy at reduced computational expense. This study presents new knowledge using a neurocomputing approach to predict the aerodynamic performance of the NACA0012 airfoil and wing, established to be accurate and reliable.

- To analyse the airfoil and wing of NACA0012, a special embedded computational intelligence framework is made using AI-BR.
- The findings obtained using the AI-BR technique are compared to the exact responses for the airfoil and wing of NACA0012 modifications.
- A detailed analysis of the AI-BR system's performance.
- Analyses of absolute error charts for the NACA0012 airfoil and wings.

The other portions of the study are organised as follows: Section 2 outlines the methods used in this work to build the dataset. Section 3 provides the theoretical framework. Section 4 provides results and analysis for all simulations. Section V summarises the findings.

2. Basic concepts and methodology

2.1. Basic concepts

Lift coefficient (C_L) and drag coefficient (C_D) are nondimensional parameters that characterize the aerodynamics of a body translating through a fluid. The lift coefficient is the ratio of lift force to dynamic pressure and reference area, and is defined by:

$$C_L = \frac{L}{\frac{1}{2}\rho V^2 A}$$

Where L is the lift force, ρ is the fluid density, V is the flow velocity, and A is the reference area (typically the wing planform area). Likewise, the drag coefficient formulates the drag force in terms of the same dynamic pressure and reference area:

$$C_D = \frac{D}{\frac{1}{2}\rho V^2 A}$$

Where D is the drag force.

2.2. Methodology

Airfoil, wing, and other aerodynamic surface design and analysis are carried out using the computer program XFLR5. The program by name "XFLR5", which is an abbreviation of "Xfoil 5" has been updated. The Xfoil and XFLR5 aerodynamics-related software programs were developed by Professor Mark Drela at the Massachusetts Institute of Technology (MIT) and are extensively used in the aerospace and aviation industries and by enthusiasts and researchers. Using XFLR5 to analyse airfoils and wings is a common method in aerodynamics and aircraft design. XFLR5 is a computational tool that enables you to undertake aerodynamic analysis, such as airfoil and wing analysis, through computational means. Below is a step-by-step process of how to use XFLR5 for this:

- *Installation:* Install and download XFLR5 on your computer. It has Windows, macOS, and Linux versions. You can download the latest version from the official XFLR5 website.
- *Create a new project:* Open XFLR5 and open a new project for your airfoil or wing analysis.
- *Airfoil selection (if analysing an airfoil):* If you're looking at an airfoil, you'll need to input the airfoil's coordinates. XFLR5 can read many airfoil file types, including .dat and .txt. You can type in the coordinates or read them from a file.
- *Wing design (if analysing a wing):* If you're examining a wing, you can create the wing geometry in XFLR5 through the integrated wing designer. Enter the wing planform, twist, dihedral, and so on.
- *Define operating conditions:* Enter the operating conditions for your simulation. These are parameters such as airspeed, α, and Reynolds number.
- *Analysis:* Conduct the analysis against your chosen airfoil or wing design and operating conditions. XFLR5 employs a vortex panel method to compute lift, drag, and other aerodynamic coefficients.
- *Results and visualisation: XFLR5 offers a variety of graphical tools to display the* results of your analysis. Pressure distributions, lift and drag polar plots, and other appropriate data can be viewed.
- *Optimisation (optional): If you are designing wings using XFLR5, you can run optimisation* studies to enhance the wing's performance. You can change wing parameters and iterate through analysing the results.
- *Export data:* If you are happy with your analysis, you can export the data and results for use elsewhere, for example, in aircraft design or in simulation software.

3. Theoretical formulation

The theoretical foundation of the present study is in the integration of artificial intelligence and computational aerodynamic simulation through a neurocomputing paradigm. The approach begins with the computation of aerodynamic data sets for the wing and NACA0012 airfoil through the use of XFLR5 software. Aerodynamic coefficients such as lift, drag, and moment under various conditions of Reynolds number and angle of attack constitute the data sets. The data is used to train an artificial neural network (ANN) with Bayesian regularisation (AI-BR). The ANN emulates the biological neurons' learning process, where nodes with connectivity process input data to generate output values. Bayesian regularisation minimises overfitting and thus promotes generalisation, allowing the trained network to remain stable even when tested on new data.

Finally, the learned model AI-BR predicts aerodynamic coefficients and performance curves, which are validated against XFLR5 and inspected via absolute error (AE) plots. This configuration demonstrates the relationship of computational fluid dynamics (data generation), machine learning (ANN training), and aerodynamic prediction (model outputs).

4. Results and discussions

Such a hypothetical neural network may be usefully compared to an artificial intelligence-based Bayesian regularisation (AI-BR) with distinguishing features that naturally link to physical and chemical properties. AI-BR has the benefit of having robust predictions and not requiring the recognition technique, which in conventional regression algorithms grows as

$O(N^2)$ in size. Strength training is challenging because an evaluation framework determines when to cease training at the optimal rate, eliminating the need for specific validation data to detect overtraining. As long as a simple architecture is offered, the network design of AI-BR is fundamentally unimportant.

This section covers the study of the airfoil and wing utilising the proposed AI-BR structure. The approach consists of two elements. First, the core discoveries of the AI-BR controller are given. The AI-BR execution approach is also used to resolve the airfoil and wing analyses. In Figure 1, a single-layer neuron arrangement is shown. Figure 2 depicts the topological organisation of AI-BR, and in Figure 3, a graphical depiction utilising numerical deterministic AI-BR is shown. With the following data setup, the AI-BR procedures are accessible in MATLAB using the "nftool" function: 80% for training, 10% for testing, and 10% for authorisation. The dataset for AI-BR is generated using XFLR5 with $Re = 4617410, \alpha = -9.90°, Mach = 0.000, NCrit = 9.0$.

Figure 1: Neuron (single-layer)

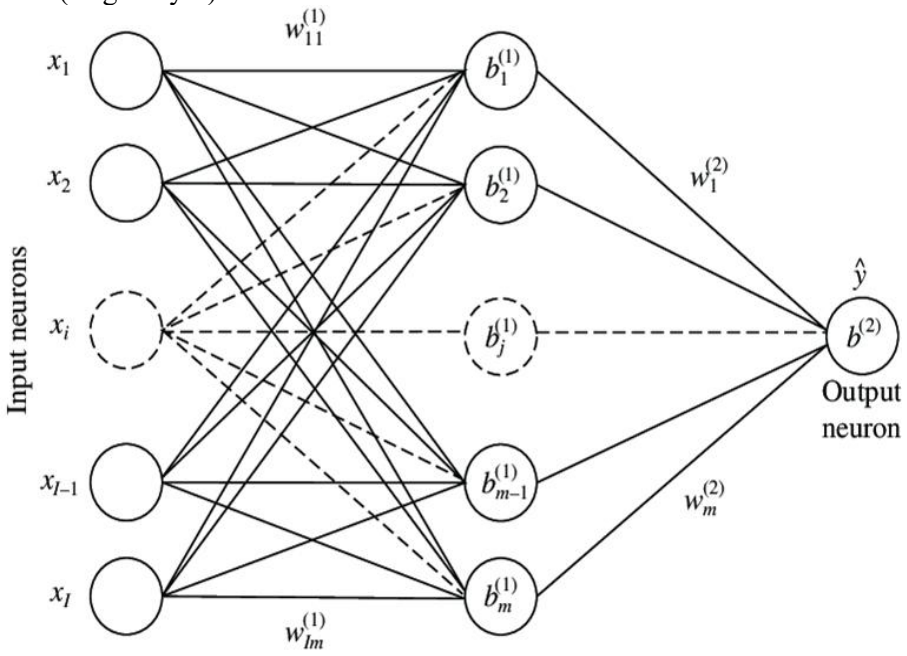

Figure 2: AI-BR topology

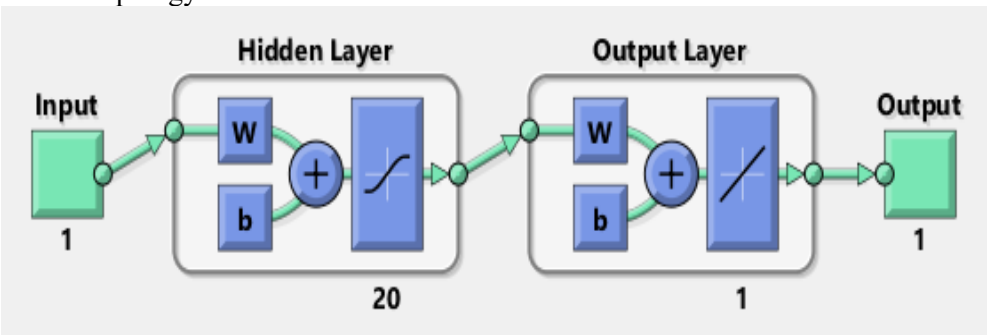

Figure 3: Graphical structure

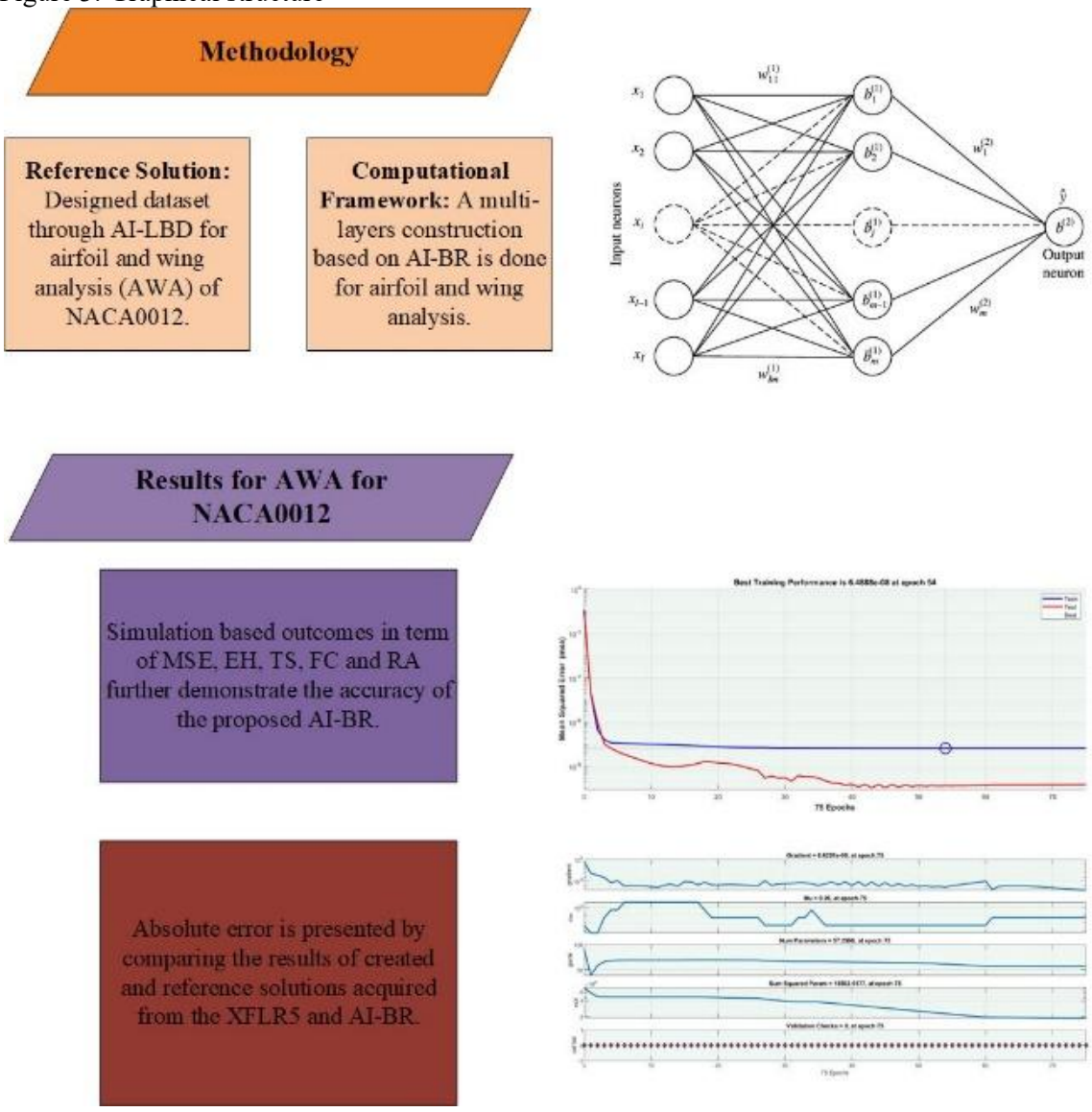

Tables (1-3) represent the simulations of airfoil analysis of NACA0012 under AI-BR for different scenarios. Table-1 is for C_D Vs C_L, Table-2 is for α vs C_L, and Table-3 is for α Vs C_D. Figures (4-6) show the graphical illustration of AI-BR for wing analysis of NACA0012 for the scenarios of Tables (1-3), respectively.

Table-1: Simulations of AI-BR for Airfoil NACA0012 based on C_L Vs C_D

Mean Square Error			Performance	Mu Parameter	Gradient	Epochs	Time
Training	Validation	Testing					
2.42111E-1	0.00000E-0	1.85034E-1	0.249	5.00E+10	0.00039	657	3s

Table-2: Simulations of AI-BR for Airfoil NACA0012 based on C_L Vs α

Mean Square Error			Performance	Mu Parameter	Gradient	Epochs	Time
Training	Validation	Testing					
8.20062E-7	0.00000E-0	8.16127E-7	8.20E-07	5.00	0.000103	1000	4s

Table-3: Simulations of AI-BR for Airfoil NACA0012 based on C_D Vs α

Mean Square Error			Performance	Mu Parameter	Gradient	Epochs	Time
Training	Validation	Testing					
6.48879E-8	0.00000E-0	1.35200E-9	6.50E-08	0.0500	8.63E-08	75	0s

Figure 4(a) shows the performance curve, which indicates that the MSE was 0.429 after 657 epochs. The estimates for gradient and mu are 0.00039 and 1E+10, respectively, according to the training state Figure 4(b). In Figure 4(c)–(e), the EH, FC, and RA are shown.

Figure 4: AI-BR simulations for airfoil NACA0012 based on C_L vs C_D

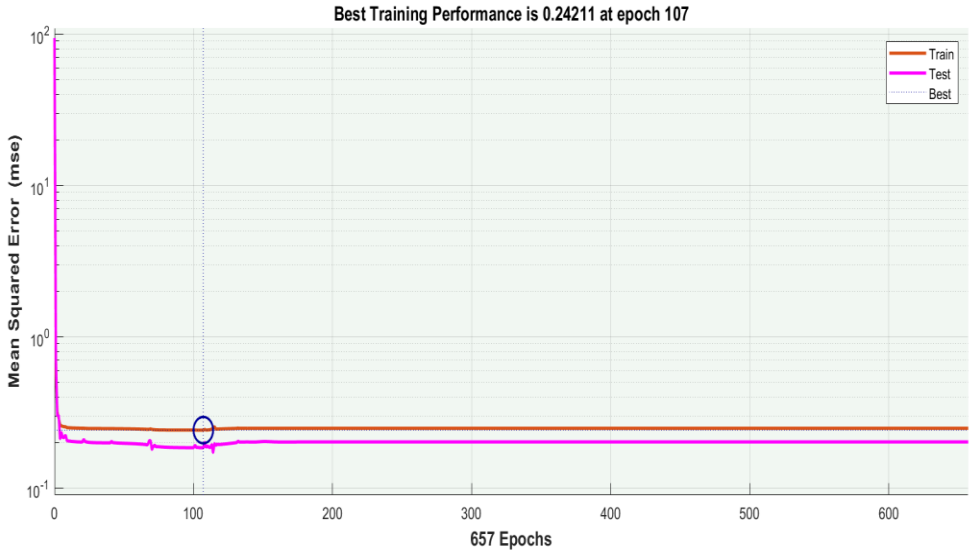

(a) MSE

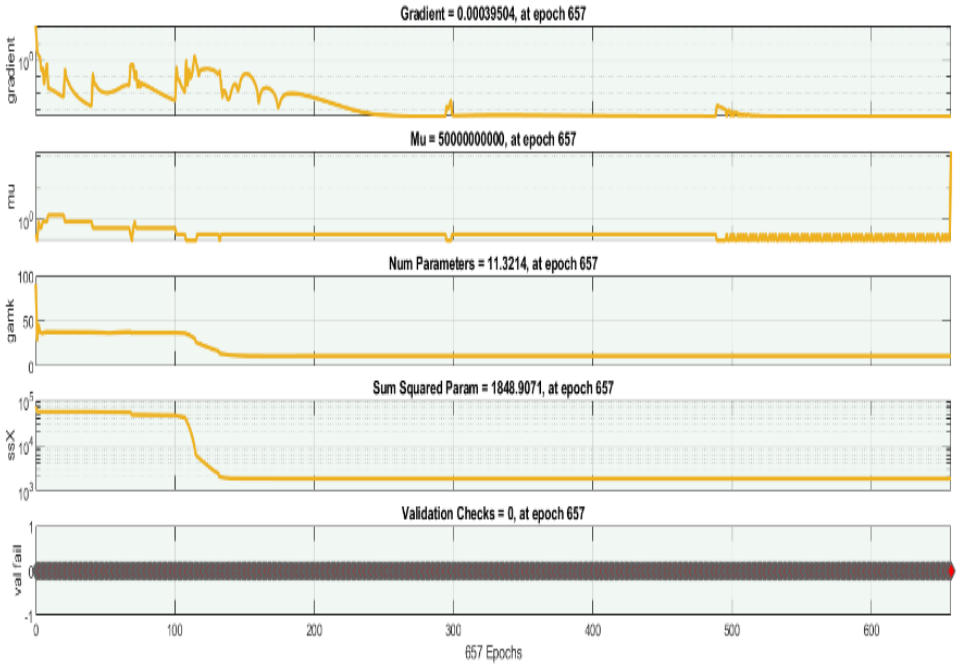

(b) TA

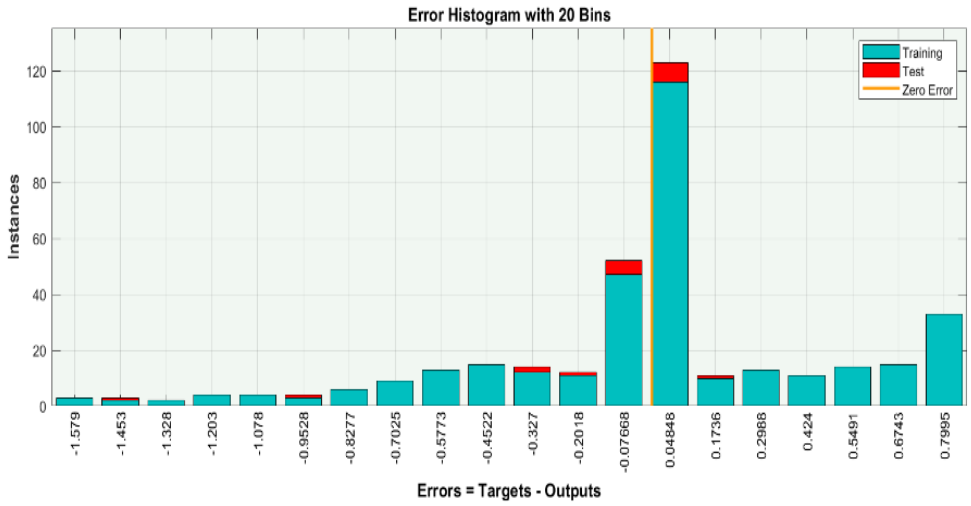
Error Histogram with 20 Bins
Training
Test
Zero Error
Instances
Errors = Targets - Outputs

(c) EH

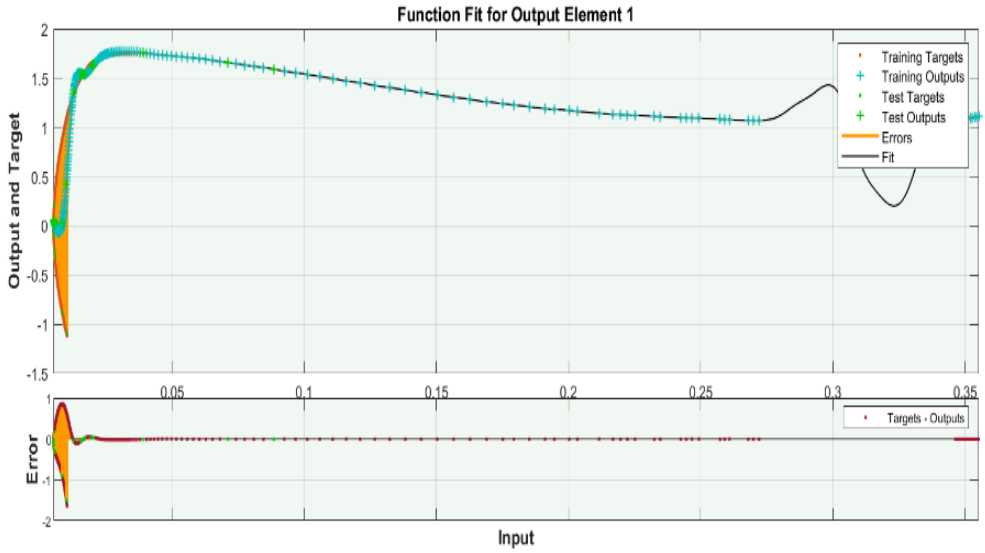
Function Fit for Output Element 1
Training Targets
Training Outputs
Test Targets
Test Outputs
Errors
Fit
Output and Target
Targets - Outputs
Error
Input

(d) FC

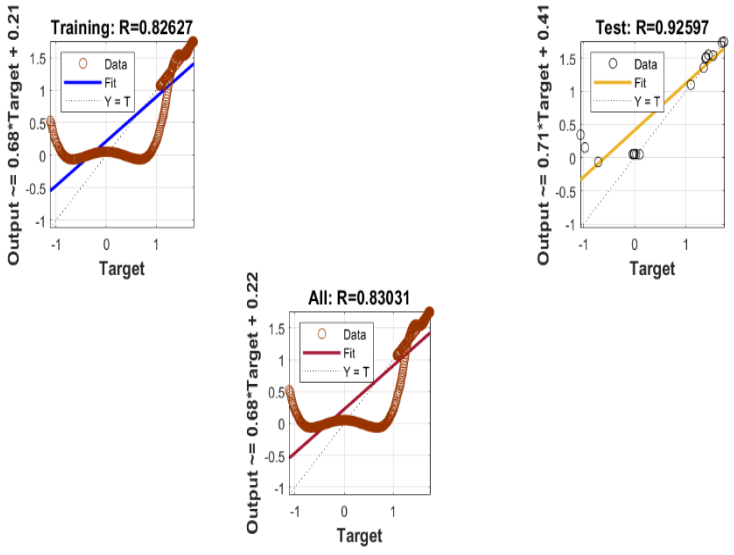
Training: R=0.82627
Test: R=0.92597
All: R=0.83031
Data
Fit
Y = T
Target

(e) RA

A performance plot in Figure 5(a) shows that the MSE after 1000 epochs is 8.20E-07. According to the training state Figure 5(b), the evaluations of gradient and mu are 0.000103 and 5, respectively. In Figure 5(c-e), the EH, FC, and RA are shown.

Figure 5: AI-BR simulations for airfoil NACA0012 based on C_L vs α

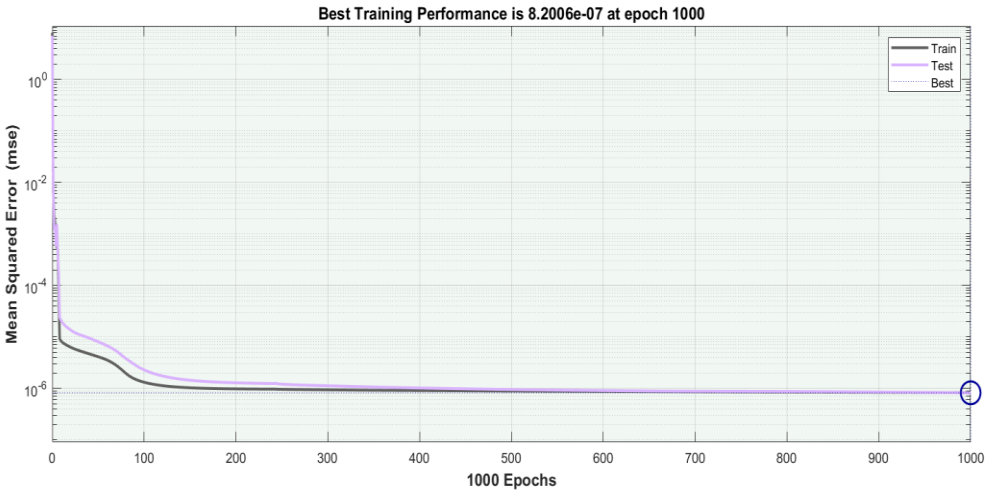

(a) MSE

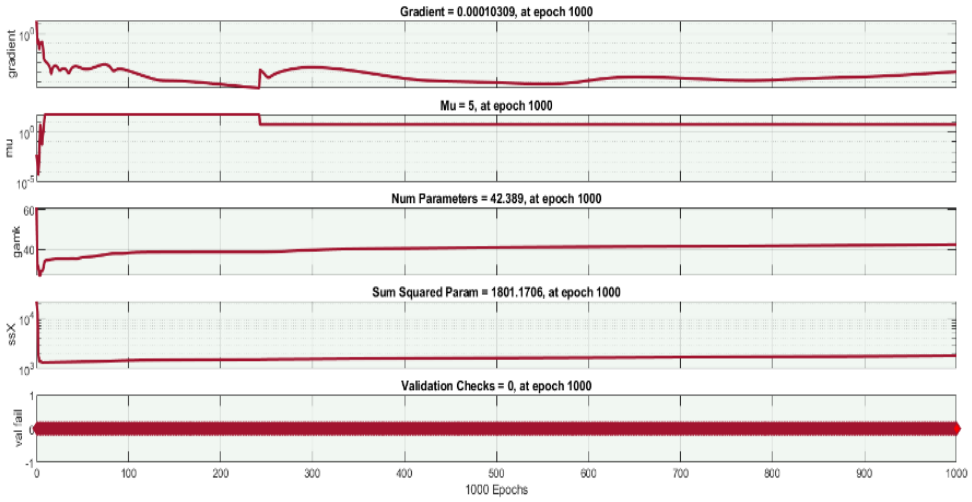

(b) TA

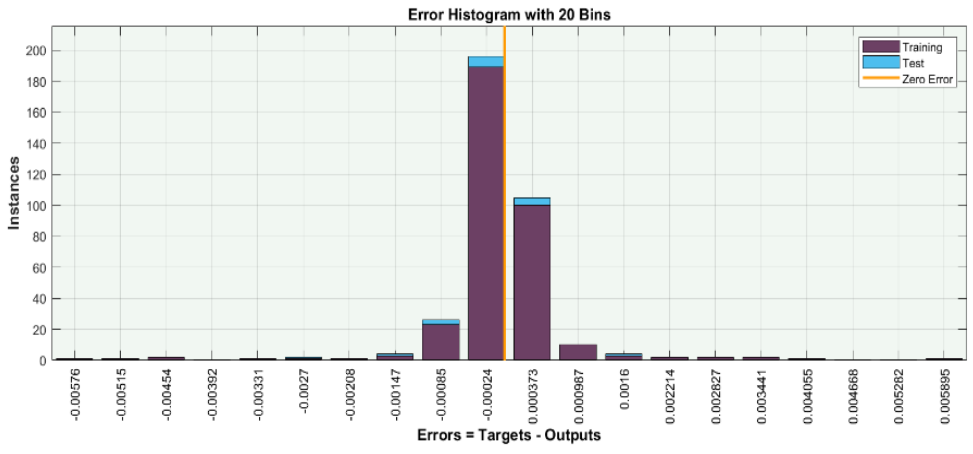

(c) EH

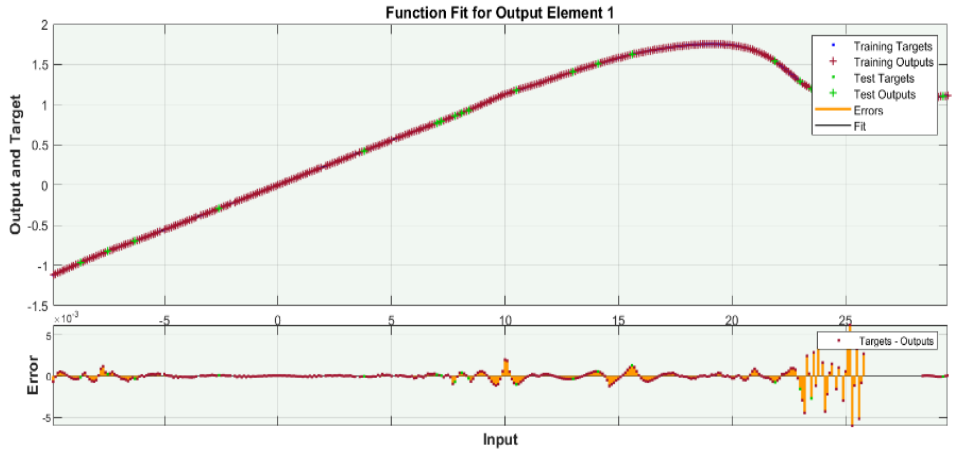

(c) FC

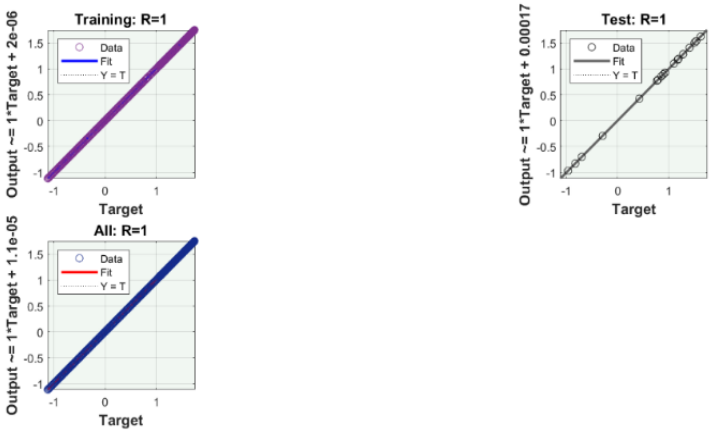

(d) RA

The performance curve in Figure 6(a) shows that the MSE after 75 epochs was 6.50E-08. The estimates for gradient and mu are 8.63E-08 and 0.05, respectively, according to the training state Figure 6(b). In Figure 6(c-e), the EH, FC, and RA are shown.

Figure 6: AI-BR simulations for airfoil NACA0012 based on C_D vs Alpha (α)

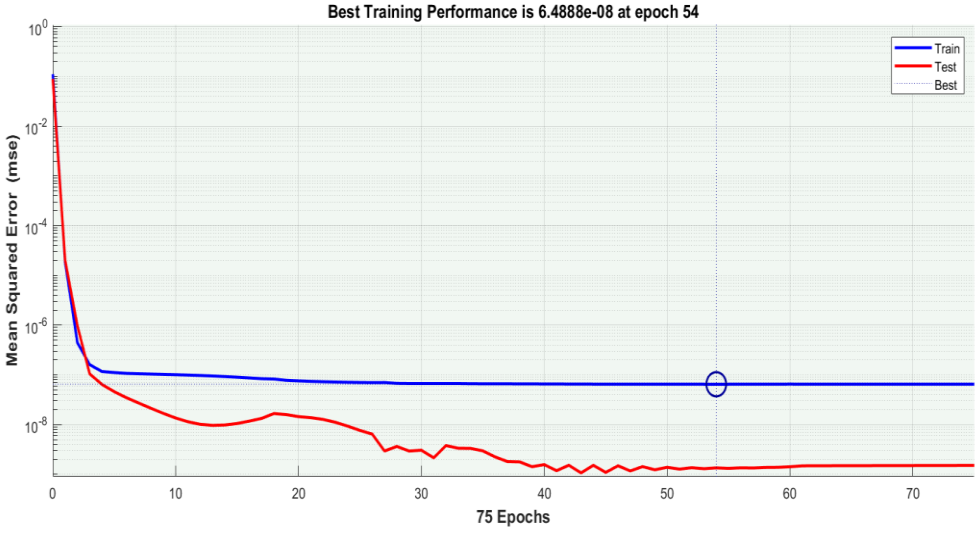

(a) MSE

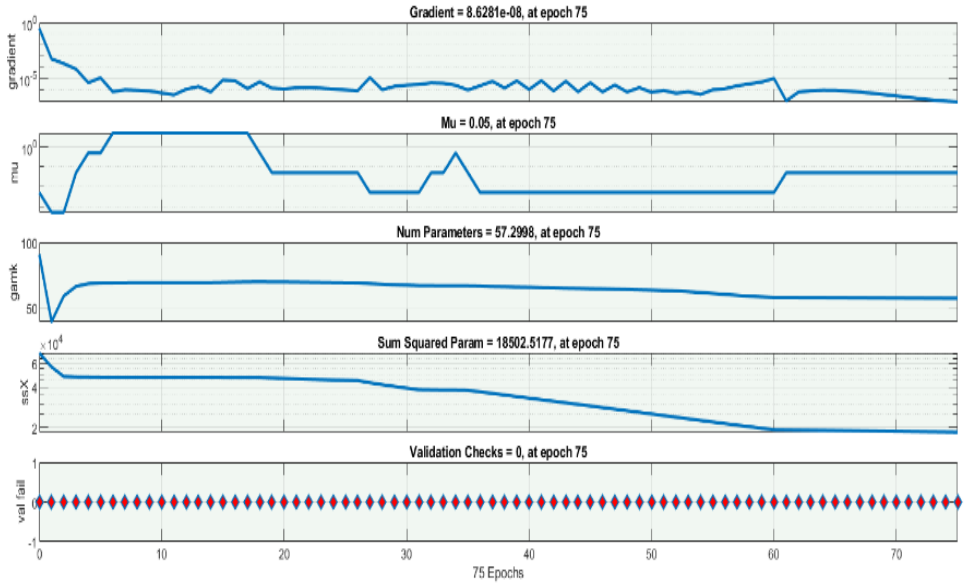
Gradient = 8.6281e-08, at epoch 75
gradient
Mu = 0.05, at epoch 75
mu
Num Parameters = 57.2998, at epoch 75
gamk
Sum Squared Param = 18502.5177, at epoch 75
ssX
Validation Checks = 0, at epoch 75
val fail
75 Epochs

(b) TA

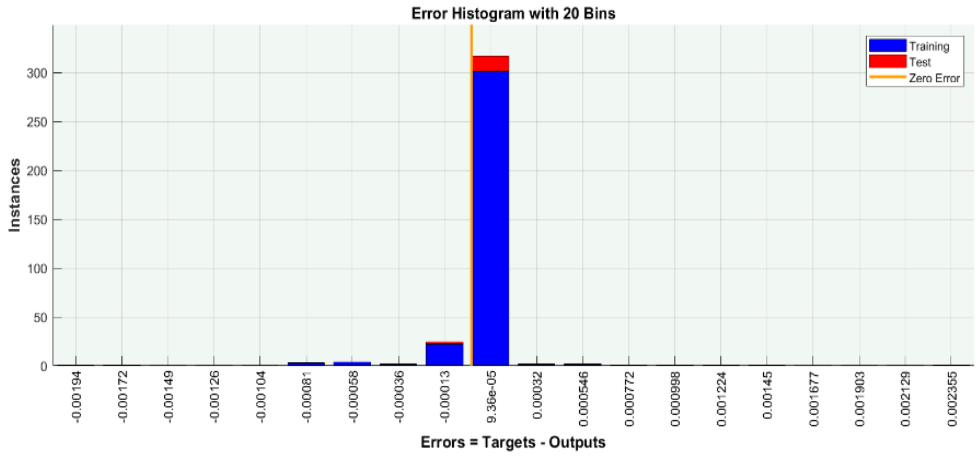
Error Histogram with 20 Bins
Training
Test
Zero Error
Instances
Errors = Targets - Outputs

(c) EH

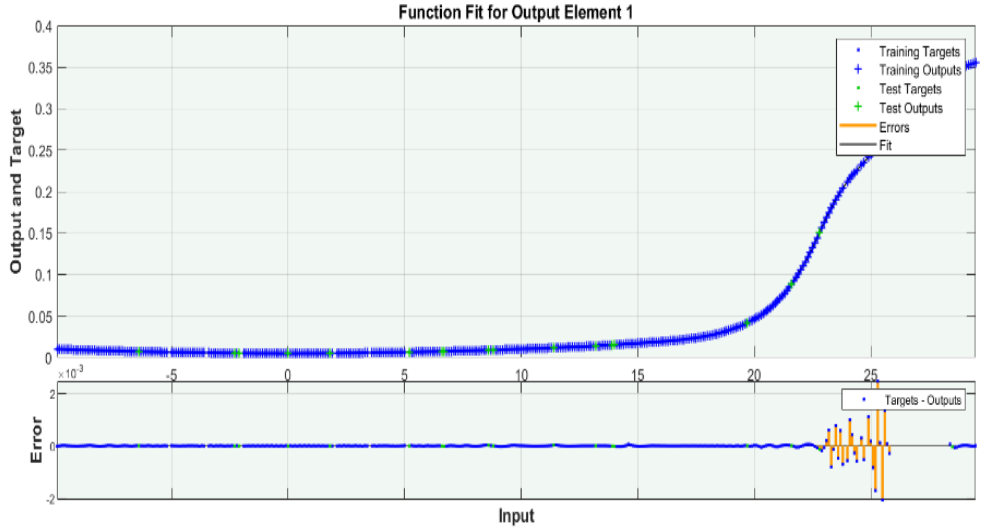
Function Fit for Output Element 1
Training Targets
Training Outputs
Test Targets
Test Outputs
Errors
Fit
Output and Target
Targets - Outputs
Error
Input

(d) FC

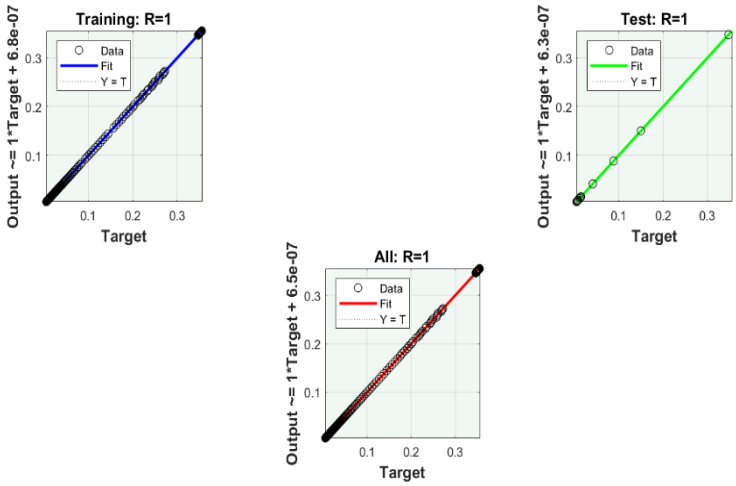

(e) RA

As indicated in Figure 7, C_L is linearly increasing with angle of attack (α) to the point of stall, after which C_L decreases steeply due to flow separation. At the same time, Cd steeply increases in the region after stall, modelling the nonlinear aerodynamic transition. Predictions of the AI-BR model are in very close agreement with XFLR5 results in both pre-stall and post-stall regimes, with slight deviations near stall. The absolute error (AE) plots (Figure 7(b, d, f)) verify that the prediction errors are within a narrow range, establishing the reliability of the framework. Such consensus identifies the ANN-BR model's capacity to emulate intricate aerodynamic phenomena at reduced computational expense relative to CFD simulations.

In detail, Figure 7(a) depicts the behaviours of $C_L\ vs. C_D$. The $C_L\ vs. C_D$ curve often displays a linear zone at small angles of attack (α), where C_l rises linearly with increasing alpha, but C_d remains relatively low. This area represents the airfoil's pre-stall behaviour. $C_{D_{max}}$ is the point on the curve where C_L attains its highest value. Accordingly, this is the α where the airfoil produces the most lift under the existing circumstances. C_D also starts to rise at this moment. The $C_L\ vs. C_D$ curve begins to depart from linearity beyond the α corresponding to $C_{L_{max}}$. In this region, also known as the stall, C_L starts to decline as C_D sharply rises. The airfoil undergoes flow separation and a decrease in lift at the stall α. The airfoil's C_L may significantly decline once the stall begins, while C_D rises.

Multiple factors, including the airfoil's shape and Reynolds number, could impact the post-stall behaviour. Figure 7(c) illustrates α vs C_L. C_L varies according to the α and follows a conventional lift curve. C_L grows linearly with alpha for small angles of attack (usually below the stall angle). The unique airfoil shape and Reynolds number determine the slope's exact value. C_L will ultimately reach its maximum value ($C_{L_{max}}$) at greater angles of attack before the airfoil stalls. NACA0012's $C_{L_{max}}$ typically ranges from 1.2 to 1.5, depending on the airfoil roughness and Reynolds number (Re). Figure 7(e) shows the behaviours of α vs C_D. Both the α and the Re have an effect on C_D. The parasitic drag (C_{D_0}) and the induced drag (C_{D_i}) are the two main parts of C_D. C_{D_i} is related to the lift produced, while C_{D_0} is the drag at zero lift.

Due to the limited generated drag at low angles of attack, C_{D_0} and C_{D_i} are both modest. C_D starts to climb significantly when the angle of attack exceeds the angle of maximum lift ($C_{L_{max}}$) because of the increase in generated drag. The airfoil is either experiencing or nearing a stall

in this area. As the flow separation increases under stall conditions, C_D can rise significantly. Figure 7 (b, d, f) shows the absolute error plots C_D vs C_L, α vs C_L and C_D vs α, $10^{1} \rightarrow 10^{-5}$, $10^{-3} \rightarrow 10^{-7}$, $10^{-3} \rightarrow 10^{-8}$ are noticed respectively. The AI-BR model predicts aerodynamic coefficients with excellent accuracy and also offers physical insight into aerodynamic performance. For example, the prediction of stall onset and post-stall behaviour is significant in UAV and wind turbine applications, where operating efficiency is highly dependent on stall characteristics.

Figure 7: Analysis of the airfoil of NACA0012 with its corresponding absolute error plots

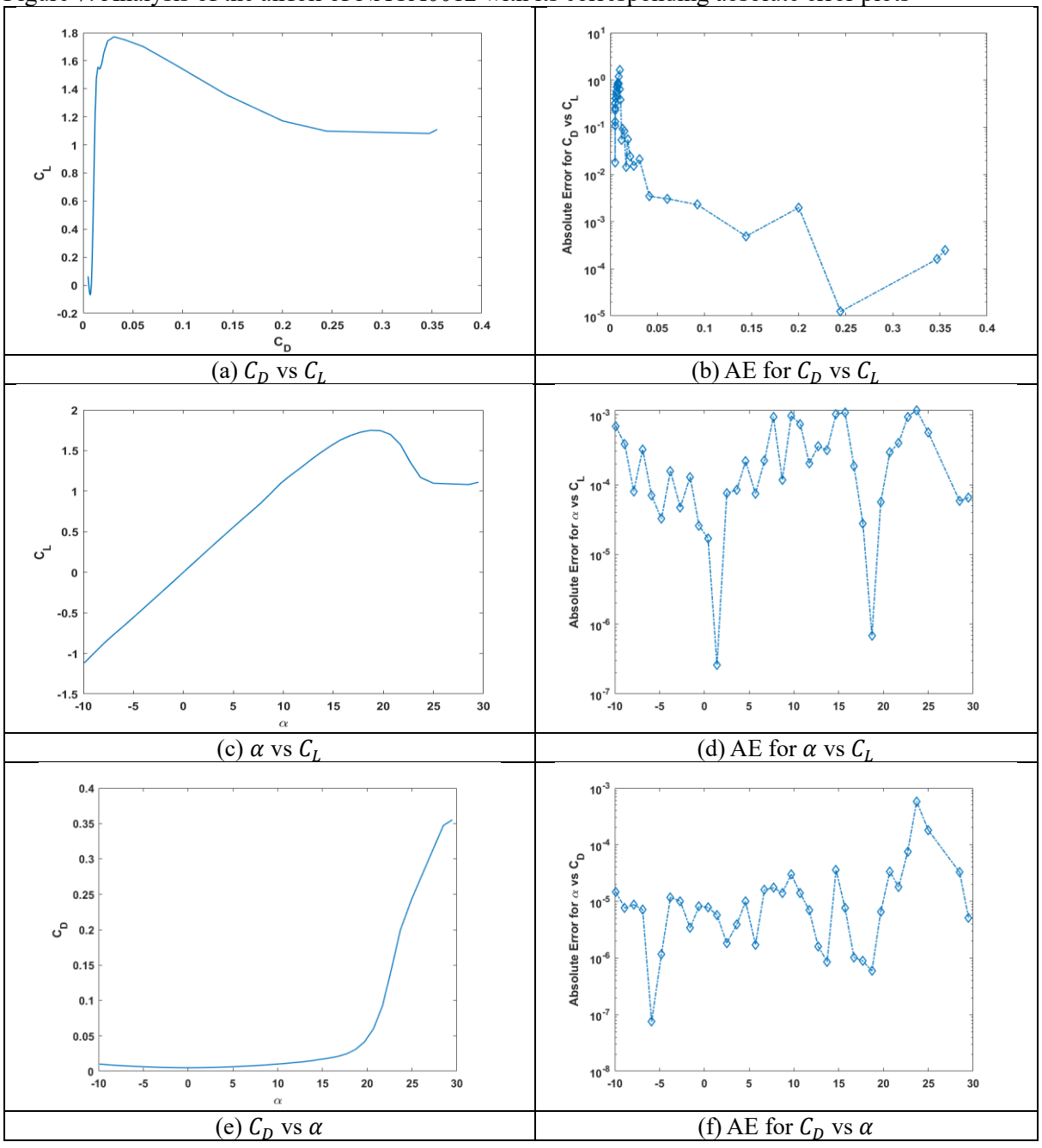

(a) C_D vs C_L (b) AE for C_D vs C_L

(c) α vs C_L (d) AE for α vs C_L

(e) C_D vs α (f) AE for C_D vs α

Table (4-7) represents the simulations of wing analysis of NACA0012 under AI-BR for different scenarios. Table-4 is for C_D vs C_L, Table-5 is for α vs C_L, Table-6 is for α vs C_L/C_D and Table-7 is for C_L vs C_L/C_D.

Table-4: Simulations of AI-BR for wing NACA0012 based on C_D vs C_L

Mean Square Error			Performance	Mu Parameter	Gradient	Epochs	Time
Training	Validation	Testing					
1.01899E-10	0.00000E-0	8.94910E-11	1.02E-10	500	7.26E-08	9	0s

Table-5: Simulations of AI-BR for wing NACA0012 based on α vs C_L

Mean Square Error			Performance	Mu Parameter	Gradient	Epochs	Time
Training	Validation	Testing					
1.62902E-9	0.00000E-0	7.63718E-8	1.63E-09	50.0	6.72E-08	825	3s

Table-6: Simulations of AI-BR for wing NACA0012 based on Alpha (α) vs C_L/C_D

Mean Square Error			Performance	Mu Parameter	Gradient	Epochs	Time
Training	Validation	Testing					
2.54468E-5	0.00000E-0	1.63285E-5	2.54E-05	50.0	0.00179	1000	5s

Table-7: Simulations of AI-BR for Wing NACA0012 based on C_L vs C_L/C_D

Mean Square Error			Performance	Mu Parameter	Gradient	Epochs	Time
Training	Validation	Testing					
3.66758E-2	0.00000E-0	5.51690E-3	0.0395	5.00E +10	0.000196	606	2s

Figures (8-11) show the graphical illustration of AI-BR for the wing analysis of the NACA0012 for the scenarios of Tables (4-7), respectively. The performance curve in Figure 8(a) reveals that the MSE was 1.02E-10 after 9 epochs. Training state Figure 8(b) gives estimates for gradient and mu of 7.26E-08 and 500, respectively. The EH, FC, and RA are displayed in 8(c-e).

According to a performance plot in Figure 9(a), the MSE at 825 epochs is 1.63E-09. The assessments of gradient and mu are 6.72E-08 and 50, respectively, as shown in the training state Figure 9(b). Figure 9(c-e) displays the EH, FC, and RA.

The performance curve in Figure 10(a) reveals that the MSE was 2.54E-05 after 1000 epochs. According to the training state Figure 10(b), the estimations for gradient and mu are 0.00179 and 50, respectively. The EH, FC, and RA are shown in Figure 10(c-e).

According to a performance plot in Figure 11(a), the MSE at 606 epochs is 0.0395. The assessments of gradient and mu are 0.000196 and 5.00E +10, respectively, according to the training state Figure 11(b). Figure 11(c-e) displays the EH, FC, and RA.

Figure 8: AI-BR simulations for wing NACA0012 based on C_D vs C_L

(a) MSE

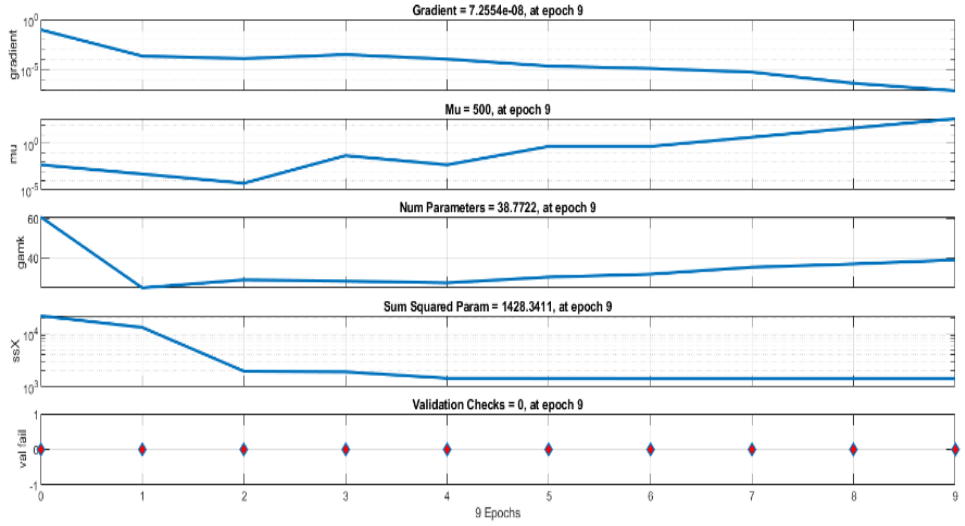

(b) TA

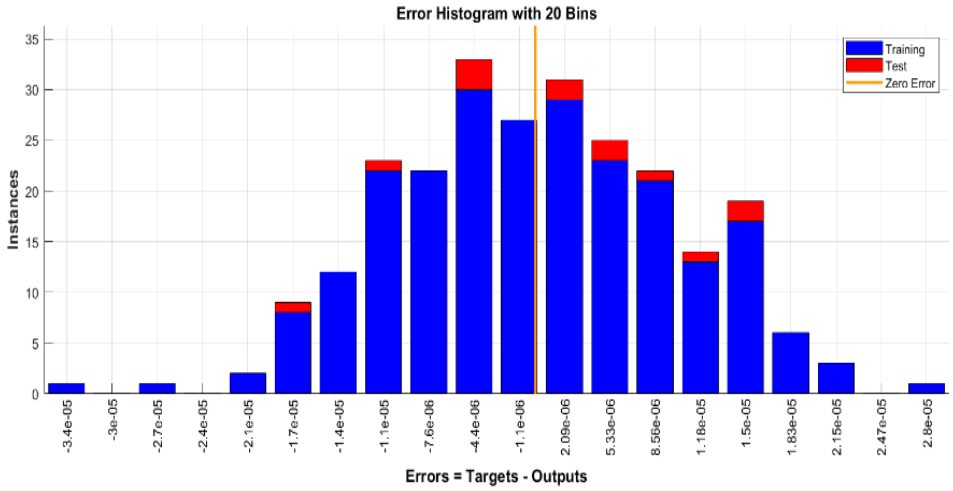

(c) EH

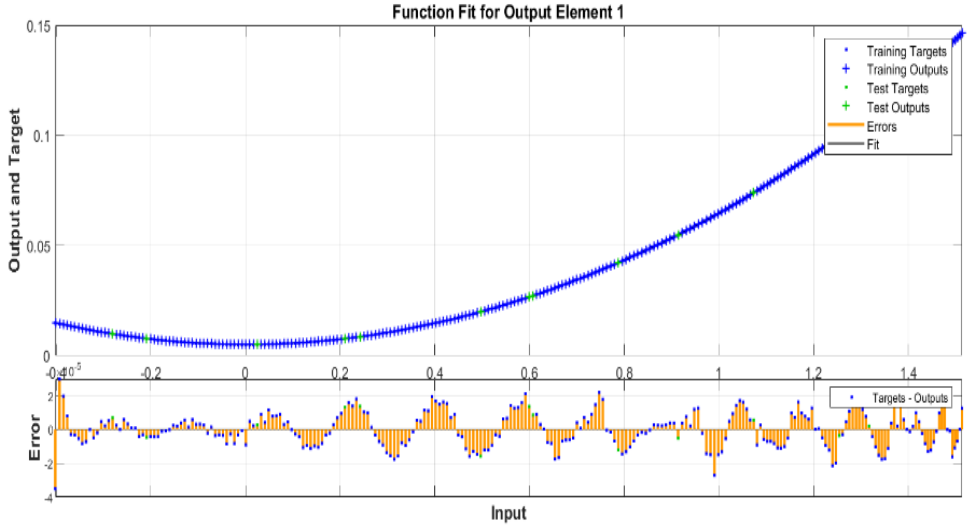

(d) FC

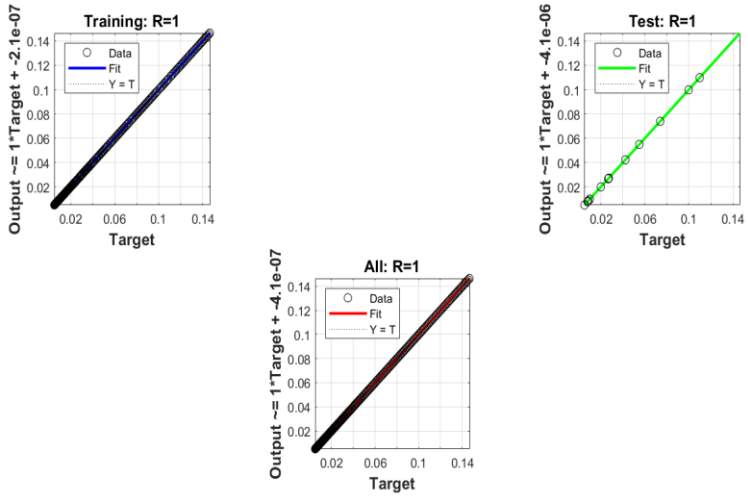

(e) RA

Figure 9: AI-BR simulations for wing NACA0012 based on Alpha (α) vs C_L

(a) MSE

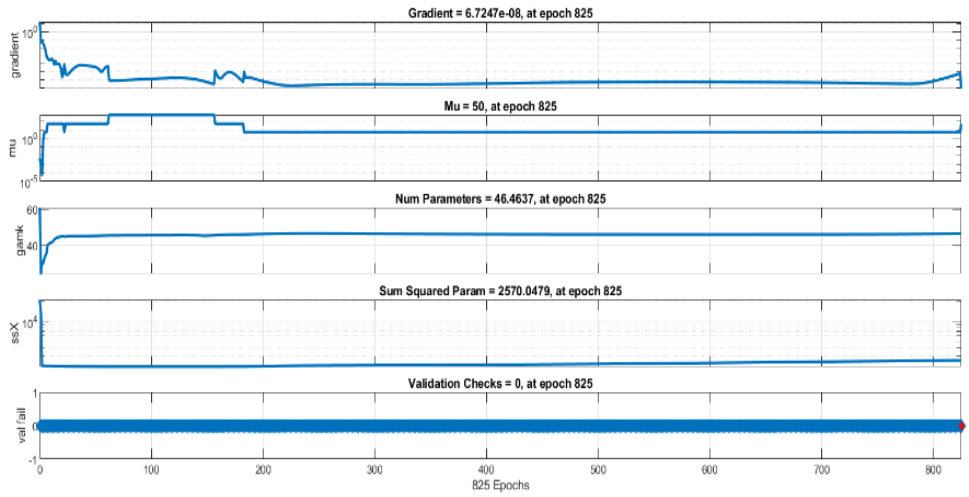
Gradient = 6.7247e-08, at epoch 825
gradient
Mu = 50, at epoch 825
mu
Num Parameters = 46.4637, at epoch 825
gamk
Sum Squared Param = 2570.0479, at epoch 825
ssX
Validation Checks = 0, at epoch 825
val fail
825 Epochs

(b) TA

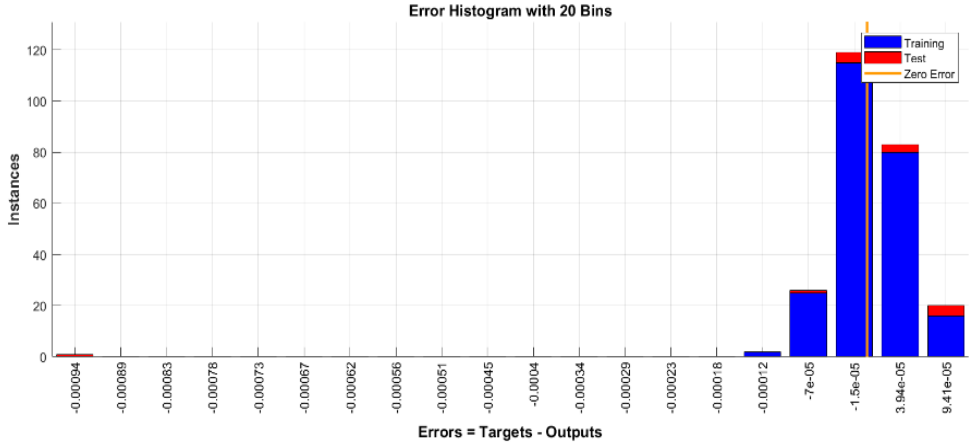
Error Histogram with 20 Bins
Training
Test
Zero Error
Instances
Errors = Targets - Outputs

(c) EH

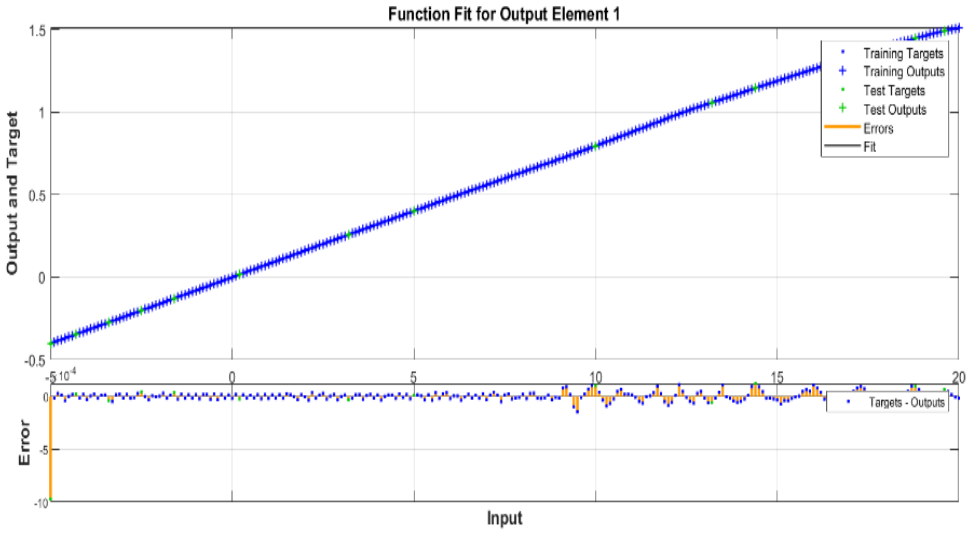
Function Fit for Output Element 1
Training Targets
Training Outputs
Test Targets
Test Outputs
Errors
Fit
Output and Target
Targets - Outputs
Error
Input

(d) FC

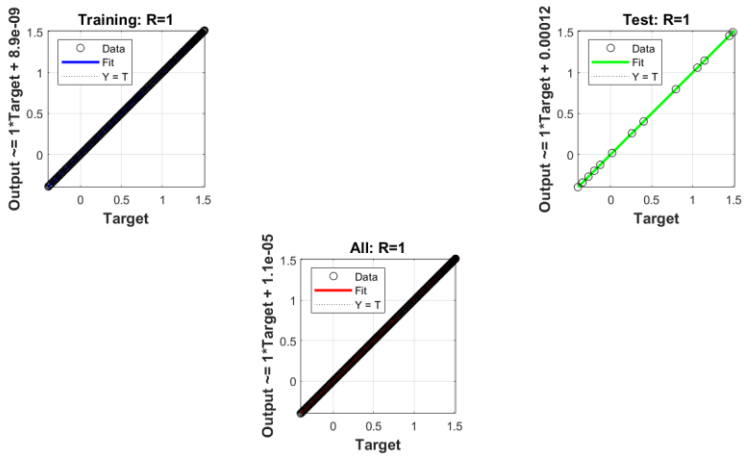

(e) RA

Figure 10: AI-BR simulations for wing NACA0012 based on Alpha (AoA) vs C_L/C_D

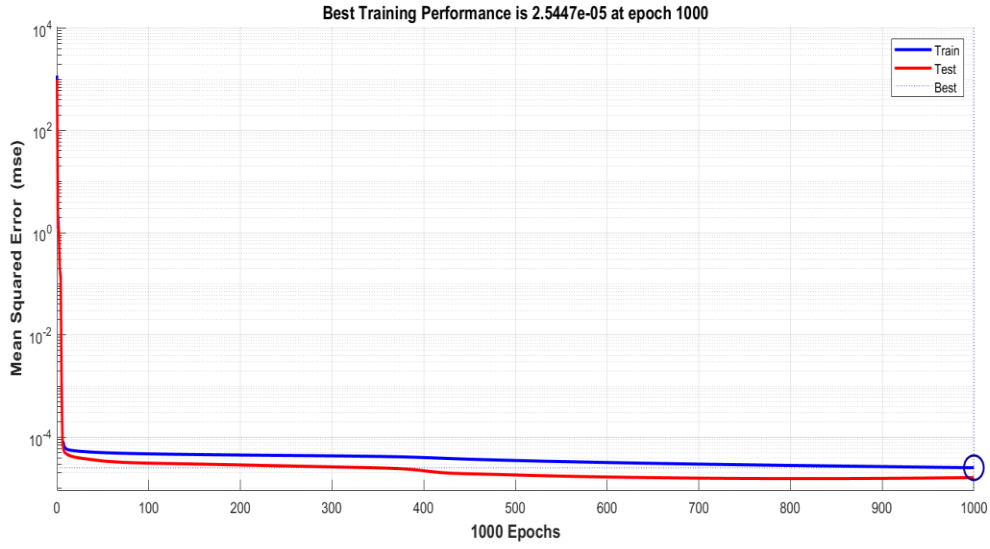

(a) MSE

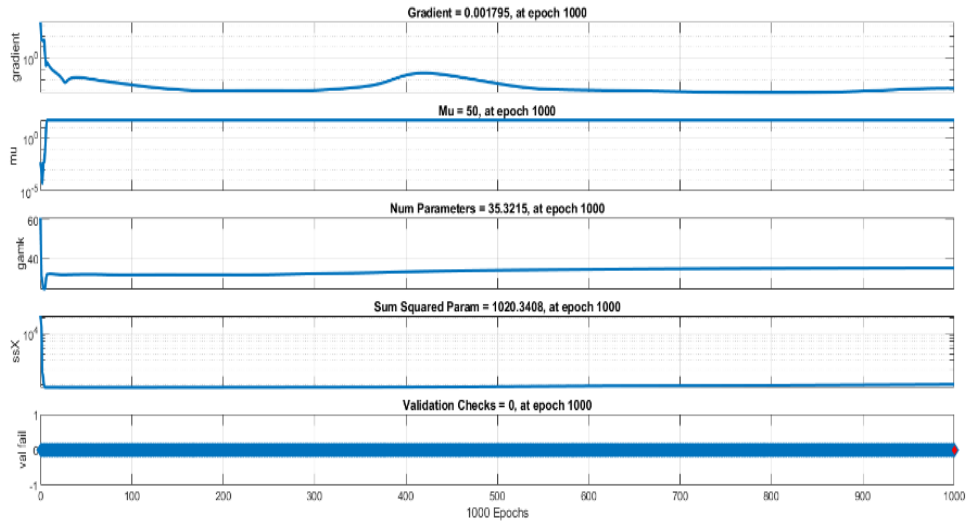

(b) TA

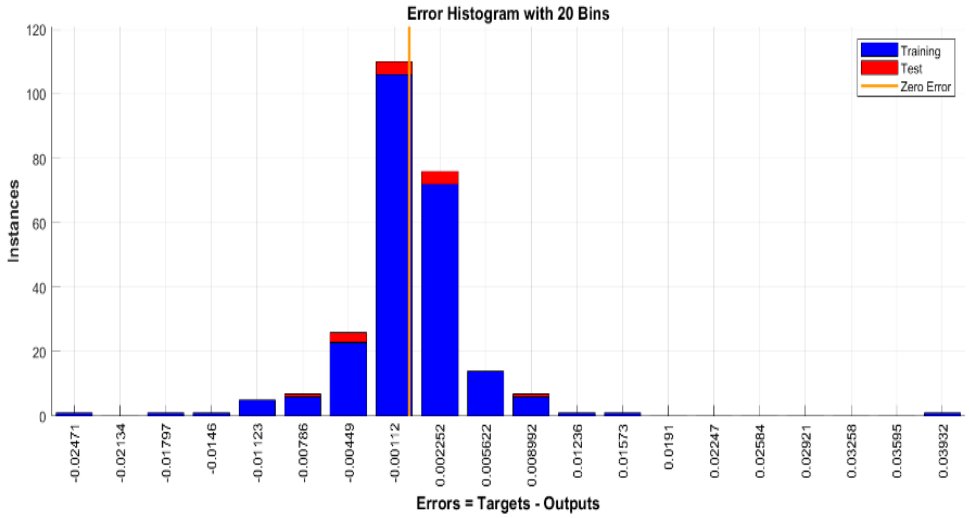
Error Histogram with 20 Bins
Training
Test
Zero Error
Instances
Errors = Targets - Outputs

(c) EH

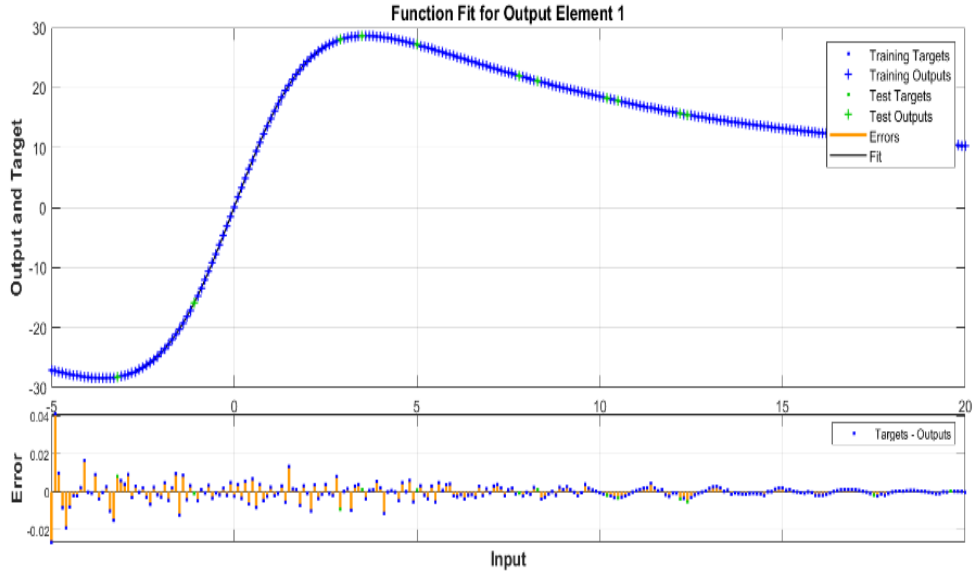
Function Fit for Output Element 1
Training Targets
Training Outputs
Test Targets
Test Outputs
Errors
Fit
Output and Target
Targets - Outputs
Error
Input

(d) FC

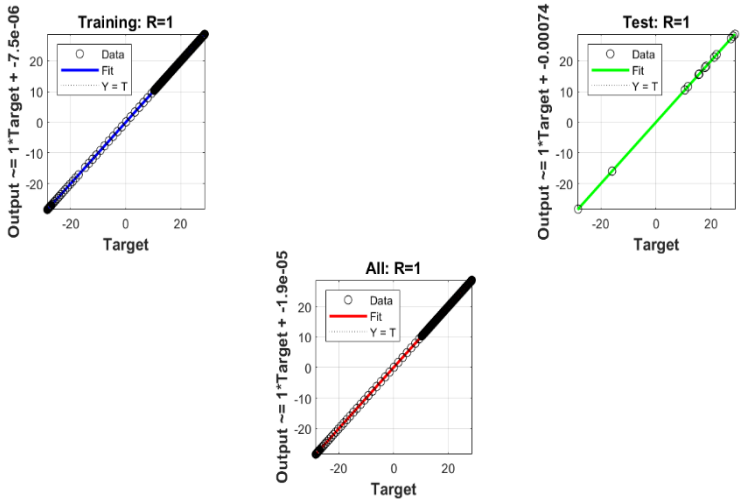
Training: R=1
Test: R=1
All: R=1
Data
Fit
Y = T
Target

(e) RA

Figure 11: AI-BR simulations for wing NACA0012 based on C_L vs C_L/C_D

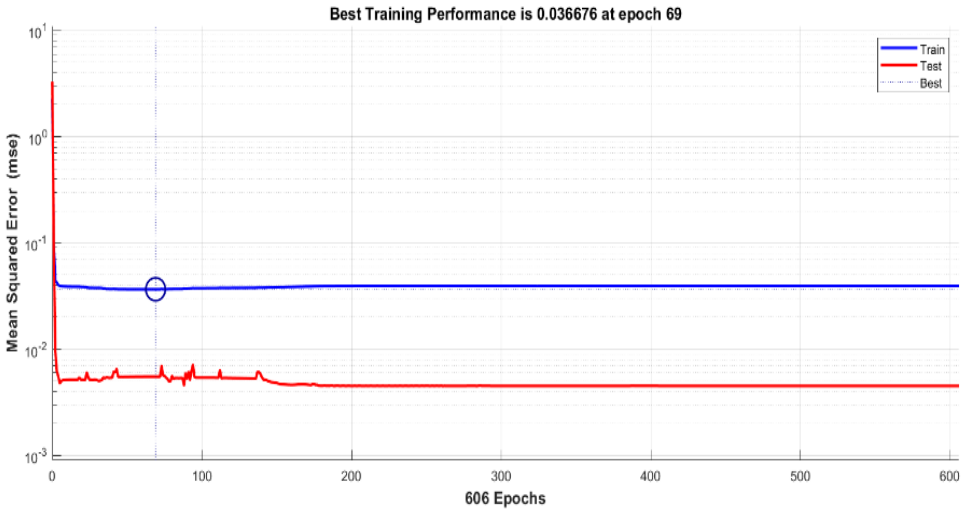

(a) MSE

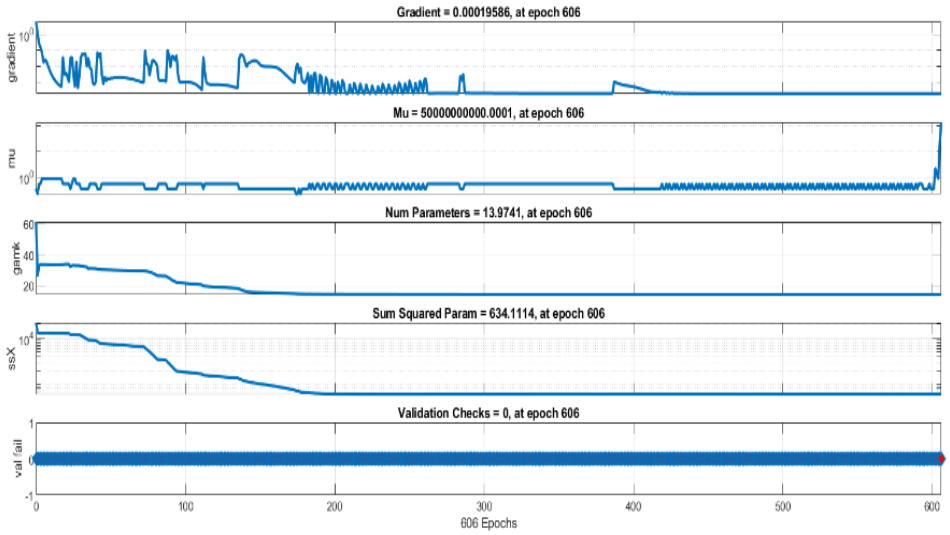

(b) TA

(c) EH

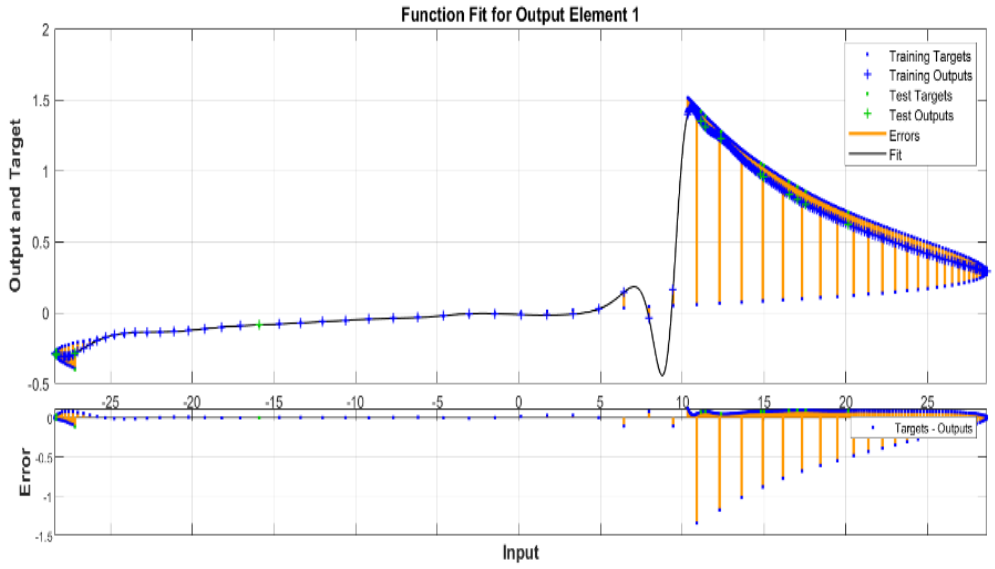

(d) FC

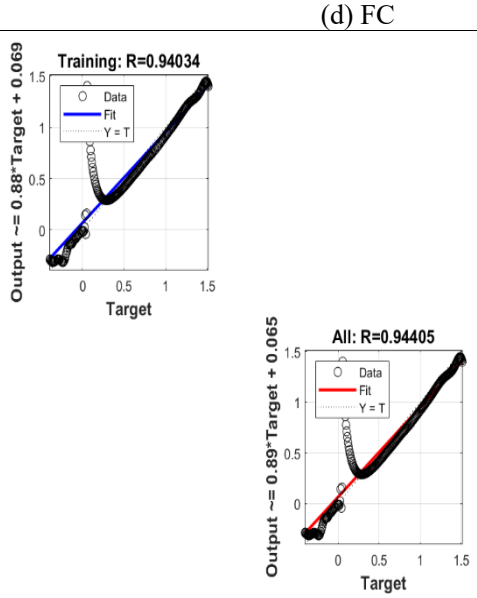

(e) RA

Figure 12(a) depicts the behaviour of the lift and drag coefficient for the wing of NACA0012. The change in the coefficients of lift (C_L) and drag (C_D) as the α increases are commonly shown on this figure. The graph shows how the lift and drag coefficients of the airfoil change with the AOA. Engineers and aerodynamicists carefully examine this representation to identify significant performance variables, such as the angle at which the airfoil reaches its maximum lift-to-drag ratio (L/D max). This AOA shows the airfoil's most effective configuration for generating lift and reducing drag. By selecting a suitable AOA that balances lift and drag according to operational requirements, one could increase the performance of the NACA0012 wing for certain applications, such as aircraft wings or wind turbine blades, by understanding the C_D vs C_L plot.

Figure 12(c) illustrates the effect of alpha with the coefficient of lift of the wing of NACA0012. The wing produces greater lift initially as alpha rises, but after a certain point, it might cause stall situations in which lift rapidly drops and drag rises, possibly leading to a loss of control.

However, C_L stands for the coefficient of lift, which measures the lift produced by the airfoil at a specific angle of attack. Engineers and pilots can better comprehend and estimate the airfoil's capacity to produce lift due to this dimensionless number. The relationship between C_L and alpha varies and sheds light on how lift changes as the α changes. When applied to the NACA 0012 airfoil, C_L normally rises with alpha until it reaches its maximum value, which happens right before the airfoil stalls. C_L quickly decreases past the crucial angle of attack.

Figure 12(e) Beginning with zero lift at alpha = 0°, the graph shows how the coefficient of lift (C_L) develops with different angles of attack (α). As alpha rises, C_L rises as well, reaching a maximum right before the airfoil stalls, or the angle of attack at which the airflow separates from the upper surface of the airfoil. Beyond that critical limit, C_L rapidly falls due to a stall, which causes lift generation to suddenly reduce. The C_L/C_D ratio on the same graph also shows the aerodynamic performance of the airfoil. This ratio initially increases as alpha increases, showing that the airfoil performs efficiently by producing higher lift with only a slight increase in drag as the angle of attack increases. However, this ratio begins to fall sharply when alpha rises beyond the point of maximum C_L/C_D. As more drag is required to produce extra lift, the airfoil becomes less efficient as its efficiency declines. The airfoil performs at its most effective at an angle of attack when the C_L/C_Dratio is highest, providing the best balance of lift and drag. In conclusion, the α vs. C_L/C_Dgraph for the NACA 0012 airfoil illustrates the optimum angle of attack and highlights the lift and drag characteristics that are angle dependent.

Figure 12(g) This graph's C_L curve, which starts at zero lift at α= 0°, shows how lift varies with changes in the angle of attack (α). The C_L value, which represents the airfoil's potential to produce lift, climbs as it increases. Before the airfoil stalls, which is the angle of attack where airflow separation takes place and lift rapidly decreases, this curve often reaches its peak. On the other hand, the C_L/C_D curve on the same graph demonstrates the aerodynamic efficiency of the airfoil. Higher C_L/C_D numbers represent an interaction between lift and drag, with higher values indicating greater efficiency in general. The C_L/C_D ratio initially climbs as increases, indicating that the airfoil operates efficiently because it creates higher lift with a comparatively small increase in drag. This ratio, however, quickly decreases as it rises beyond the angle of maximum C_L/C_D. This decrease shows that the airfoil reduces efficiency because it now takes a bigger increase in drag to produce more lift. The optimum flight position of the airfoil, in which it attains an optimum compromise between lift and drag and defines its maximum aerodynamic efficiency, is given by the angle of attack corresponding to the maximum C_L/C_D. ratio.

This concept is crucial for the design and refinement of aircraft wings to meet specific performance requirements. Therefore, engineers can use the graph of C_L vs. C_L/C_D. for NACA0012 wings in order to identify how lift and aerodynamic performance vary with variations in α. The research conducted under XFLR5 is more accurate at defining the aerodynamics of the airfoil, as a smaller absolute error means a closer fit between the predicted and observed values. Particularly, the extreme MSE reduction during the first few hundred epochs clearly suggests that the network required fewer iterations to reach its best weights, which manifests how Bayesian regularisation effectively guides the learning process. On the other hand, a greater absolute error indicates that the expected and experimental findings differ significantly, necessitating more study or confirmation. Figure 12(b, d, f) shows the absolute error plots C_D vs C_L, α vs C_L, α vs C_L/C_D and C_L vs C_L/C_D , $10^{-4} \rightarrow 10^{-8}$, $10^{-3} \rightarrow 10^{-6}$, $10^{-1} \rightarrow 10^{-4}$, $10^{0} \rightarrow 10^{-3}$ are noticed respectively.

Figure 12: Analysis of the wing of NACA0012 with its corresponding absolute error plots

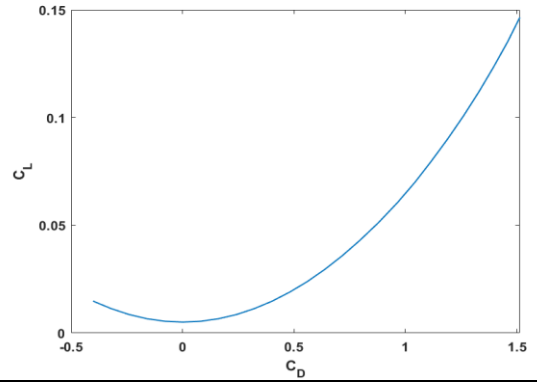

(a) $C_D\ vs\ C_L$

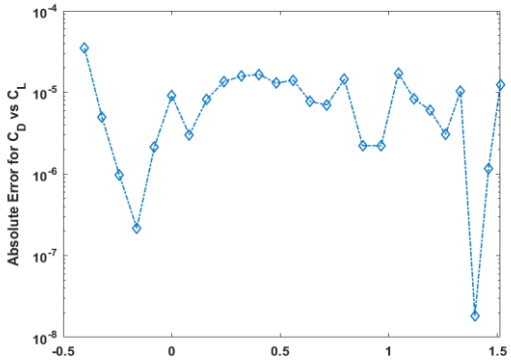

(b) AE for $C_D\ vs\ C_L$

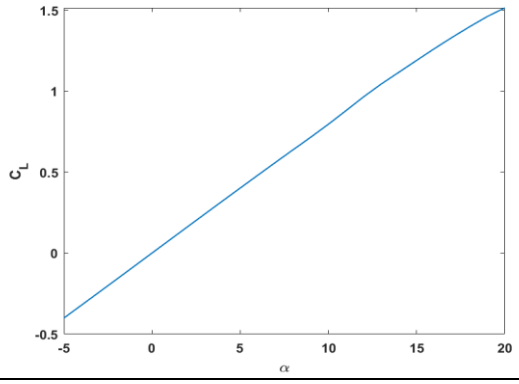

(c) $\alpha\ vs\ C_L$

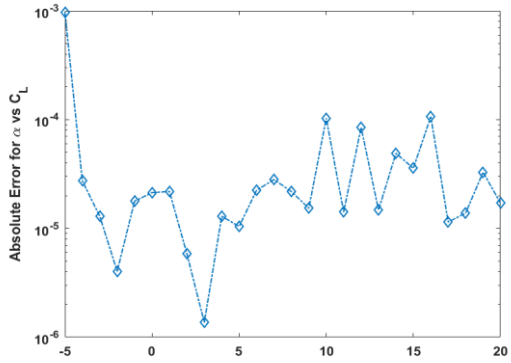

(d) AE for $\alpha\ vs\ C_L$

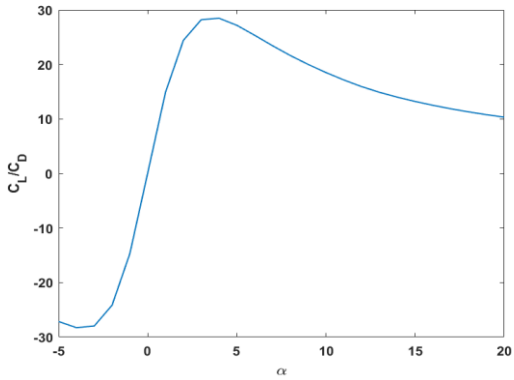

(e) $\alpha\ vs\ C_L/C_D$

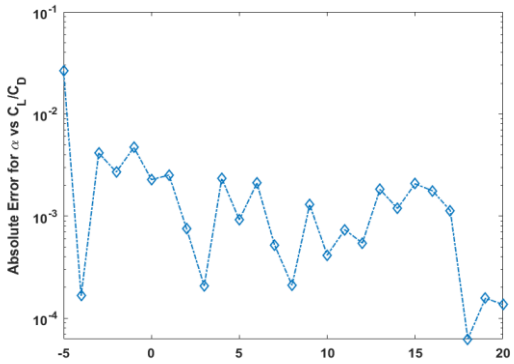

(f) AE for $\alpha\ vs\ C_L/C_D$

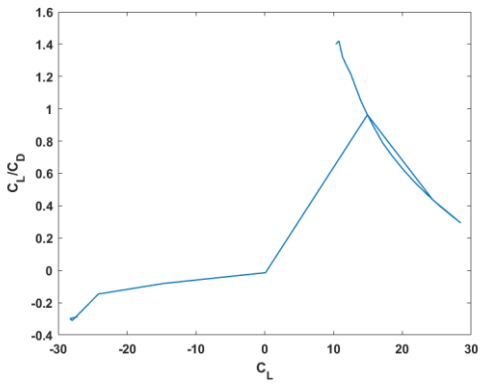

(g) $C_L\ vs\ C_L/C_D$

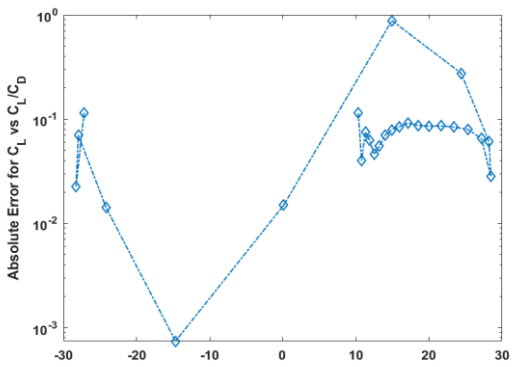

(h) AE for $C_L\ vs\ C_L/C_D$

The comparison of the AI-BR predictions with the XFLR5 simulations reveals some interesting observations. First, the AI-BR model consistently yielded smooth convergence curves with extremely low mean square error (MSE) values for both airfoil and wing cases. This suggests that the model learned to represent the underlying aerodynamic relationships without oscillations or instability in training. Secondly, the regression plots exhibit nearly linear relationships between outputs and target values with R-values closely approaching unity. This high agreement guarantees that the ANN did not merely memorise the training set but learned an average mapping that can be applied to make correct predictions for unseen test and validation cases. Such generalisation becomes critical when the framework is being extrapolated to other Reynolds numbers, airfoil geometries, or flow conditions beyond those selectively given within the training set. Third, plots of absolute error (AE) reveal further insight into the quality of the framework. The distribution of error remained confined for most operating conditions, with departures slightly larger in regions close to stall. This is expected since the nonlinear flow separation and vortex dynamics close to stall are more challenging to model than pre-stall linear conditions. But the AI-BR model was successful in approximating such nonlinear transitions to fair accuracy, following the XFLR5 reference curve very closely.

Finally, in the wing analysis, the AI-BR system successfully modelled three-dimensional aerodynamic features, including downwash and induced drag. The predicted lift-to-drag ratio trend was in good correlation with XFLR5 results, detecting the angle of maximum aerodynamic efficiency accurately. This capability is particularly useful for design optimisation, as the identification of the optimum operating angle of attack is paramount in realising optimal performance in real-world applications such as UAVs and wind turbines. AI-BR's capability to estimate these aerodynamic trends with lower computational costs indicates its potential as a surrogate model for preliminary aerodynamic design and optimisation studies. This study presented a neurocomputing approach employing artificial neural networks with Bayesian regularisation (AI-BR) to investigate the aerodynamic performance of the NACA0012 airfoil and wing.

5. Conclusion and future suggestions

Training and validation datasets generated by XFLR5 were integrated into the AI-BR model, and findings indicated high predictive accuracy at low absolute values of error. Regression analysis, histograms of errors, and mean square error plots certified the stability, reliability, and robustness of the suggested approach. Furthermore, the high correlation between ANN predictions and XFLR5 simulations validated the ability of the framework to simulate aerodynamic characteristics under different flow conditions. As a fast, accurate, and computationally lightweight alternative to traditional CFD and experimental methodologies, this contribution highlights the potential of neurocomputing for aerodynamic modelling.

Even though this study demonstrates the effectiveness of neurocomputing with Bayesian regularisation in solving the aerodynamic characteristics of the NACA0012 airfoil and wing, there are various opportunities for future research. First, the method can be applied to other airfoil families and three-dimensional wing shapes, such as high-lift and cambered profiles, in order to confirm its general utility. Second, the inclusion of experimental wind tunnel data as well as XFLR5 simulations would increase model validity even further and offer greater validation against actual aerodynamic measurements. Third, optimisation algorithms with higher-order complexity, like genetic algorithms or particle swarm optimisation, could be coupled with the AI-BR model to aid in airfoil and wing design optimisation for particular

applications. In addition, real-time application of this framework is to be investigated for unmanned aerial vehicles (UAVs), drones, and wind turbine blades, where fast aerodynamic predictions are necessary for adaptive control and energy efficiency.

Declaration of conflict of interest:

The author(s) declared no potential conflicts of interest(s) with respect to the research, authorship, and/or publication of this article.

Funding:

The author(s) received no financial support for the research, authorship and/or publication of this article.

Publisher's Note:

IDEA Publishers Group (NASIJ IDEA-PG) stands neutral with regard to jurisdictional claims in the published maps and institutional affiliations.

References

Abbasi, A. Z., Rafiq, A., Alshammari, B. M., & Jaghdam, I. H. (2025a). An advanced image encryption scheme based on generalised triangle group and neural networks. *Ain Shams Engineering Journal, 16*(8), 103488. https://doi.org/10.1016/j.asej.2025.103488

Abbasi, A. Z., Aamir, M., Sattar, M., Abdullah, N., Abdennaji, T. S., Alshammri, B. M., & Kolsi, L. (2025b). Modelling and prediction of 3D Carreau Fluid behaviour using machine learning for Cattaneo Christov double diffusion with variable conductivity. *Case Studies in Thermal Engineering*, 106302. https://doi.org/10.1016/j.csite.2025.106302

Aamir, M., Alshehery, S., Abbasi, A. Z., Sohail, M. U., Khan, N., Mesloub, A., ... & Kolsi, L. (2025). Analysis for 3D thermal conducting micropolar nanofluid via artificial neural network. *The European Physical Journal Plus, 140*(2), 100. https://link.springer.com/article/10.1140/epjp/s13360-025-06022-8

Abbott, I. H., & von Doenhoff, A. E. (1959). Including a summary of Airfoil data. *New York*.

Ananda, G. K., Sukumar, P. P., & Selig, M. S. (2015). Measured aerodynamic characteristics of wings at low Reynolds numbers. *Aerospace Science and Technology, 42*, 392-406. https://doi.org/10.1016/j.ast.2014.11.016

Anand, A., Safdar, M. M., Marepally, K., & Baeder, J. D. (2025). A comprehensive review of neural network training approaches for airfoil design and optimization. *In AIAA SCITECH 2025 Forum* (p. 0271). https://doi.org/10.2514/6.2025-0271

Boulkeraa, T., Ghenaiet, A., Mendez, S., & Mohammadi, B. (2014). A numerical optimization chain combining computational fluid dynamics and surrogate analysis for the aerodynamic design of airfoils. *Proceedings of the Institution of Mechanical Engineers, Part G: Journal of Aerospace Engineering, 228*(11), 1964-1981. https://doi.org/10.1177/0954410013506159

Camacho, E. A., Silva, A. R., & Marques, F. D. (2025). Predicting airfoil dynamic stall loads using neural networks. *Aerospace Science and Technology, 165*, 110466. https://doi.org/10.1016/j.ast.2025.110466

Chen, Q., Sabir, Z., Mehmood, M. A., & Baskonus, H. M. (2025). A machine learning radial basis deep neural network for solving the fractional chaotic financial system. *Journal of Computational and Applied Mathematics,* 116936. https://doi.org/10.1016/j.cam.2025.116936

Cuerno-Rejado, C., López-Martínez, G., Escudero-Arahuetes, J. L., & López-Díez, J. (2001). Experimental aerodynamic characteristics of NACA 0012 airfoils with simulated glaze and rime ice. *Proceedings of the Institution of Mechanical Engineers, Part G: Journal of Aerospace Engineering*, *215*(4), 229-240. https://doi.org/10.1243/0954410011533211

Del Pino, C., Parras, L., Felli, M., & Fernandez-Feria, R. (2011). Structure of trailing vortices: Comparison between particle image velocimetry measurements and theoretical models. *Physics of Fluids*, *23*(1). https://doi.org/10.1063/1.3537791

Fincham, J. H. S., & Friswell, M. I. (2015). Aerodynamic optimisation of a camber morphing aerofoil. *Aerospace Science and Technology*, *43*, 245-255. https://doi.org/10.1016/j.ast.2015.02.023

Karay, M., Sabir, Z., Akkilic, A. N., & Bulut, H. (2025). A stochastic neural network for the numerical solutions of the nonlinear fractional order Zika virus model using reservoirs and human motion. *Computational Biology and Chemistry*, 108629. https://doi.org/10.1016/j.compbiolchem.2025.108629

Laitone, E. V. (1997). Wind tunnel tests of wings at Reynolds numbers below 70,000. *Experiments in fluids*, *23*(5), 405-409.

Ngo, H. T., & Barlow, L. E. (2002). *U.S. Patent No. 6,394,397*. Patent and Trademark Office.

Sabir, Z., & Abdelkawy, M. A. (2025). A novel combination of sigmoid and radial basis neural networks for the monkeypox transmission system. *Engineering Applications of Artificial Intelligence, 158*, 111512. https://doi.org/10.1016/j.engappai.2025.111512

Sheldahl, R. E., & Klimas, P. C. (1981). *Aerodynamic characteristics of seven symmetrical airfoil sections through 180-degree angle of attack for use in aerodynamic analysis of vertical axis wind turbines* (No. SAND-80-2114). Sandia National Labs., Albuquerque, NM (USA).

Wassing, S., Langer, S., & Bekemeyer, P. (2025). Physics-informed neural networks for inviscid transonic flows around an airfoil. *Physics of Fluids, 37*(8). https://doi.org/10.1063/5.0276518